J. Coat. Technol. Res.
https://doi.org/10.1007/s11998-019-00263-w

Development of functionalized SiO_2–TiO_2 reinforced cardanol and caprolactam modified diamine based polybenzoxazine nanocomposites for high performance applications

T. Lakshmikandhan, Arumugam Hariharan, K. Sethuraman, Muthukaruppan Alagar

Abstract In the present work, three types of polybenzoxazines were synthesized using caprolactam-based diamine (CPA-NH_2) and formaldehyde with different phenols, namely 4-fluorophenol, cardanol, and phenol, under appropriate experimental conditions. The molecular structure of the benzoxazine monomers was confirmed by FTIR, ^1H, and ^{13}C NMR spectroscopic techniques. Polybenzoxazines were obtained through ring-opening polymerization of benzoxazine monomers, and their formation was confirmed by FTIR spectroscopy. The elemental composition and morphological behavior of polybenzoxazines were characterized by SEM-EDAX and AFM techniques. The naturally occurring cardanol- and caprolactam-based diamine (CPA-NH_2)-based benzoxazine was selected for detailed studies. The synthesized SiO_2–TiO_2 nanohybrid reinforcement was functionalized with 3-aminopropyltrimethoxysilane (3-APS) and reinforced with cardanol-based benzoxazine (CPBz) monomer. The resulted nanocomposites were studied for their corrosion protection behavior against mild steel surface along with thermomechanical (TGA and DMA) and morphological (SEM, XRD, and TEM) properties. The results obtained from electrochemical impedance analysis indicate that the 5 wt% of F–SiO_2–TiO_2 of reinforced CPBz exhibits an effective corrosion-resistant behavior toward surface of steel specimen than that of other samples.

Keywords Cardanol-based benzoxazine, Functionalized SiO_2–TiO_2, Thermomechanical properties, Nanocomposites, Storage modulus, Glass transition temperature, Anticorrosion properties

Introduction

Thermosetting resins are widely used in high-performance applications, in the form of coating materials, caulks, adhesives, insulating materials, and construction materials in electronics, automobile, and aerospace industries. Thermosetting epoxy resins are generally used in coatings to prevent corrosion of metal substrates due to their good mechanical properties, strong adhesion, high crosslink density, and excellent chemical resistance. However, the epoxy resins used for protective coating are known to be less efficient in an aqueous environment, since the moisture can penetrate into the interface between the organic coatings and the substrates.[1,2] To overcome these problems, new types of addition-cure phenolic systems, namely polybenzoxazines (PBzs)-based phenolic resins, were developed recently.

Polybenzoxazines are obtained from benzoxazine monomers through ring-opening thermal polymerization of the oxirane ring in the absence of a catalyst. These resins possess many advantages over conventional phenolic resins such as near-zero shrinkage upon curing, low moisture absorption, high char yield, no catalysts required for curing, having long shelf life, and no release of by-products. In addition, they also possess good thermomechanical properties, better dielectric

Electronic supplementary material The online version of this article (https://doi.org/10.1007/s11998-019-00263-w) contains supplementary material, which is available to authorized users.

T. Lakshmikandhan,
Department of Chemistry, Bharath Institute of Higher Education and Research, Selaiyur, Chennai 600073, India

A. Hariharan, M. Alagar (✉)
Polymer Engineering Laboratory, PSG Institute of Technology and Applied Research, Neelambur, Coimbatore, Tamil Nadu 642061, India
e-mail: mkalagar@yahoo.com

K. Sethuraman,
Polymer Composite Laboratory, Department of Chemical Engineering, Anna University, Chennai 600025, India

Published online: 12 September 2019

properties, and resistance to radiation, corrosion, flame, and chemicals.[3–8]

At present, renewable resource material-based polymeric products have attracted the attention of both academic and industrial researchers due to fast depletion of petroleum feedstock and environmental issues. In this context, cardanol is considered as one of the well-known phenolic compounds obtained as a renewable biosource and it is a by-product obtained from processing of cashew nutshell. The chemically modified cardanol and its products exhibit an excellent performance and are also converted into a number of specialty polymers.[9–12] Cardanol-based polybenzoxazines (CPBz) have received much research attention because they possess high thermal stability, high char yield, high glass transition temperature (T_g), good mechanical and better dielectric properties, low water absorption, super-hydrophobic behavior, and excellent solubility in low-boiling organic solvents. These properties are comparable and better than those of conventional phenolic resins.[13] In the present work, caprolactam-based diamine (CPA-NH_2) was used as one of the reactants to synthesize cardanol-based benzoxazine monomer, since it possesses the high thermomechanical properties and is suitable for the fabrication of polymer composites because of its resilient and flexible structure (–NH–CO–) and capability of crosslinking with benzoxazine matrix.[14] Recently, it was reported that the coatings obtained from benzoxazines and nanoreinforcements such as TiO_2,[15,16] SiO_2,[17–19] ZnO,[20,21] ZrO_2,[22], and Fe_2O_3[23] possess excellent environmental properties. Among them, the TiO_2 and SiO_2 inorganic reinforcements exhibit good anticorrosion properties, high thermal stability, nontoxic nature, excellent mechanical properties, and competitive cost. These characteristics make polybenzoxazines become an excellent material for high-performance industrial uses including corrosion-resistant applications.

In the present work, an attempt has been made to prepare three different types of polybenzoxazines using a skeletally modified caprolactam-based diamine with varying nature of phenols (phenol, 4-fluorophenol, and cardanol) and their properties were characterized using modern analytical techniques. Benzoxazine prepared using caprolactam-modified diamine with cardanol was reinforced with varying weight percentages of aminosilane-functionalized silica–titania (F-SiO_2–TiO_2), and their properties were analyzed using modern analytical technologies. Data resulted from different studies are discussed and reported.

Experimental

Materials

Analytical grades of 4-fluorophenol, phenol, caprolactam, *N*-methyl 2-pyrrolidone (NMP), alkali hypophosphate, chloroform, ethanol, nitric acid, hydrofluoric acid, acetic acid, isopropanol, chloroform, and paraformaldehyde were purchased from SRL, India. 4,4-Diaminodiphenylmethane (DDM) was obtained from Ciba-Geigy Ltd., India. Cardanol was obtained from Satya Cashew Chemicals Pvt. Ltd., Chennai, India. Titanium tetraisopropoxide (TTIP) and tetraethyl orthosilicate (TEOS) were purchased from Sigma-Aldrich.

Synthesis of caprolactam diamine (CPA-NH_2)

Caprolactam diamine (CPA-NH_2) was synthesized as per our earlier report.[14,24] In a two-necked round-bottomed flask equipped with a condenser, 100 ml NMP, 10 g (0.0883 mol) of caprolactam, 7.8 g (0.0442 mol) of 4,4´-diaminodiphenylmethane, and 5 mg of alkali hypophosphate catalyst were added. The mixture was allowed to react at 160°C for 24 h with efficient agitation to facilitate the completion of reaction.[25] The resulted product was filtered by separation and purified (yield 85%) (Scheme 1).

Synthesis of phenol-based benzoxazine (PBz)

To the caprolactam diamine (5 g, 0.011 mol) in chloroform, formaldehyde (1.4 g, 0.047 mol) was added and stirred for 30 min at 0°C. Subsequently, 2.07 g of phenol (0.023 mol) was added to the reaction mixture and stirred for overnight at 70°C. After the completion of reaction, the reaction product was extracted with ethyl acetate and washed with 2 N NaOH and water. Finally, the organic layer was concentrated to obtain the product with 92% yield. The formation of product (benzoxazine) is presented in Scheme 2.

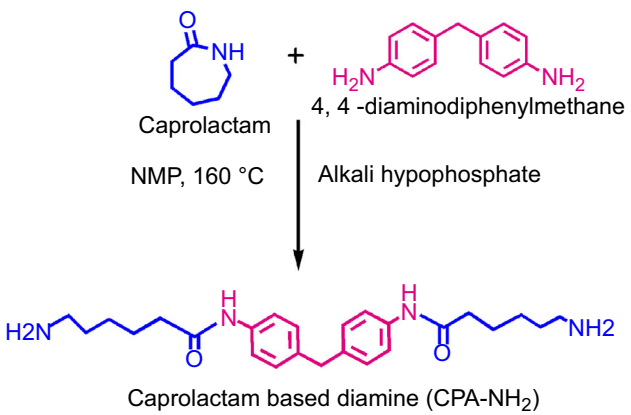

Scheme 1: Synthesis of caprolactam-based diamine (CPA–NH_2)

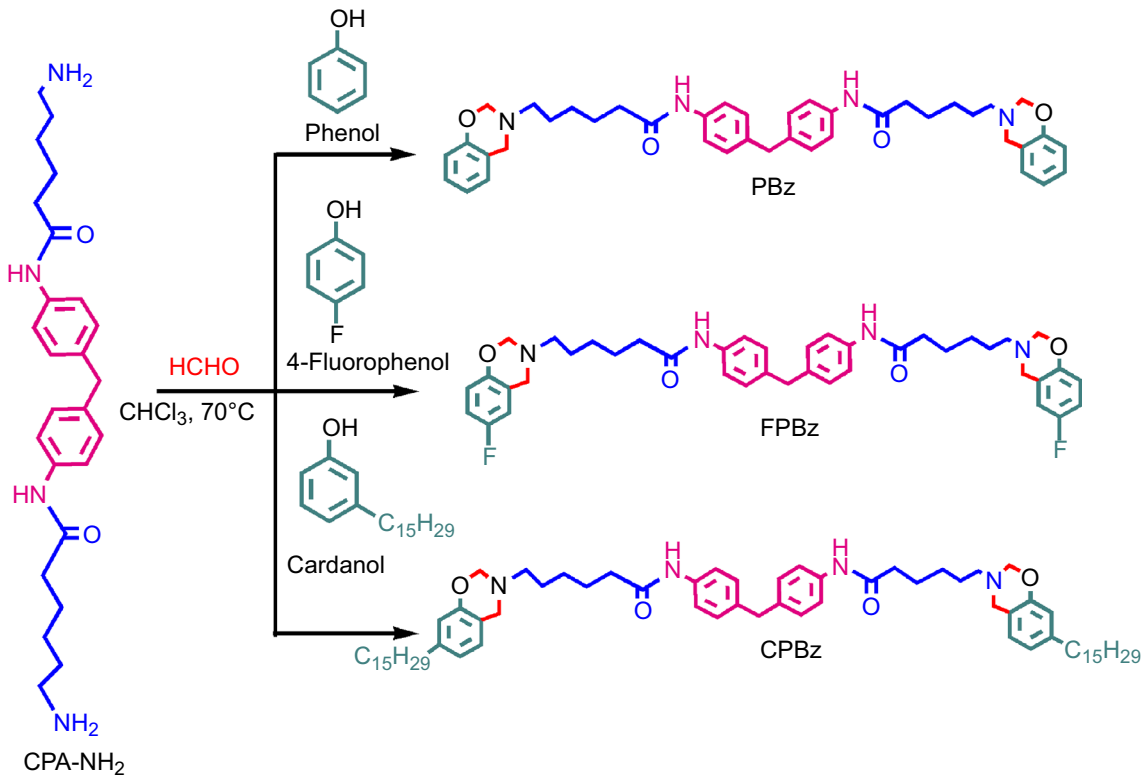

Scheme 2: Synthesis of three different types of benzoxazines

Synthesis of 4-fluorophenol-based benzoxazine (FPBz)

To the caprolactam amine (5 g, 0.011 mol) in chloroform, formaldehyde (1.4 g, 0.047 mol) was added and stirred for 30 min at 0°C. Subsequently, 2.46 g of 4-fluorophenol (0.023 mol) was added to the reaction mixture and stirred overnight at 70°C. After the completion of reaction, the reaction product was extracted with ethyl acetate and washed with 2 N NaOH and water. Finally, the organic layer was concentrated to obtain product with 90% yield, and the formation of benzoxazine is presented in Scheme 2.

Synthesis of cardanol-based benzoxazine (CPBz)

To the caprolactam amine (5 g, 0.011 mol) in chloroform, formaldehyde (1.4 g, 0.047 mol) was added and stirred for 30 min at 0°C (ice-cold condition). Subsequently, 7.42 g of cardanol (0.023 mol) was added to the reaction mixture and stirred for overnight at 70°C. After the completion of reaction, the reaction product was extracted with ethyl acetate and washed with 2 N NaOH and water. Finally, the organic layer was concentrated to obtain benzoxazine with 90% yield (Scheme 2).

Synthesis of SiO_2 nanosilica

Nanosilica SiO_2 was prepared by the hydrolysis of tetraethyl orthosilicate (TEOS). A mixture of ethanol, water, nitric acid (1 N), and hydrofluoric acid (3 wt%) was prepared in the volume ratio of 14:7:1:1, and 2.3 parts of the same were added to one part of TEOS in a polypropylene beaker which was magnetically stirred for an hour at room temperature and then at 60°C until the formation of gel. The gel obtained was then dried at 110°C for 16 h, well ground, and kept for calcination at 600°C for 5 h to obtain the nanoparticles of silica.[26]

Preparation of SiO_2–TiO_2 and functionalized SiO_2–TiO_2 nanoparticles

SiO_2–TiO_2 nanohybrid materials were prepared by sol–gel method which involved the acidic hydrolysis of titanium tetraisopropoxide (TTIP) over the synthesized SiO_2 substrate. This was done by the slow addition of solution A which is a mixture of TTIP and isopropanol in the weight ratio of 1:2.4 to solution B which is a mixture of acetic acid, isopropanol, and water in the weight ratio of 1:4:0.33 under continuous mechanical stirring to ensure maximum homogeneity of the solution. After the complete addition of the solution A to the solution B, the temperature of the

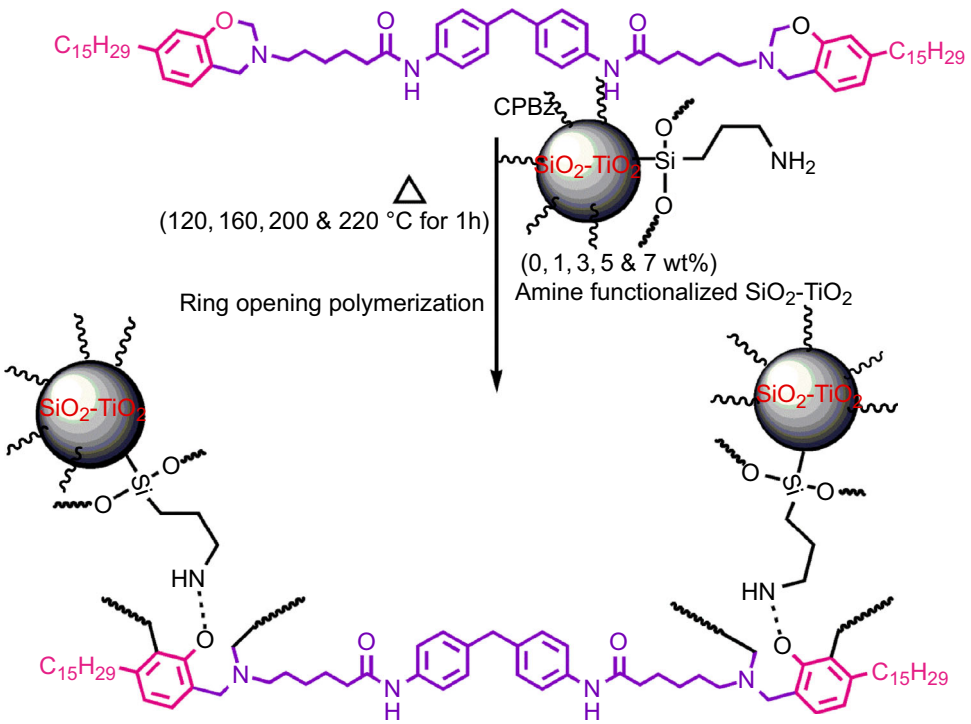

Scheme 3: Preparation of F-SiO_2–TiO_2-reinforced CPBz nanocomposites

system was increased slowly to 75°C and stirring was continued until most of the solvent evaporated, and the contents of the system could no longer be stirred. The resultant wet product was dried at 110°C for about 16 h and calcined at 500°C for 6 h to obtain SiO_2–TiO_2 hybrid.[27]

Surface functionalization of SiO_2–TiO_2 was achieved through the reaction between 3-aminopropyltriethoxysilane and the hydroxyl groups available on the surface of nano-SiO_2–TiO_2. Typically, 2 g of nano-SiO_2–TiO_2 was dispersed in 40 ml ethanol under ultrasonication for 30 min, and 2 ml of 3-aminopropyltriethoxysilane was added and refluxed at 110°C for 12 h under constant stirring. The resulted aminosilane-functionalized nano-SiO_2–TiO_2 was collected by filtration, dried under vacuum for 12 h, and preserved for further use.[24]

Preparation of neat CPBz and F-SiO_2–TiO_2-reinforced CPBz nanocomposites

The cardanol-based benzoxazine and varying weight percentages (1, 3, 5, and 7 wt%) of F-SiO_2–TiO_2 were dissolved in $CHCl_3$ solvent separately with constant mechanical stirring for 2 h. After the complete dissolution, the solutions were transferred to the respective Petri dish, were thermally treated at 70°C for overnight to evaporate the solvent, and were then cured stepwise at 120, 160, 200, and 220°C for 1 h each to obtain dark brown-colored composite films (Scheme 3).[14,25]

Surface preparation of the mild steel specimens

Mild steel specimens (of composition C—0.04%; Si—0.01%; Mn—0.17%; P—0.002%; S—0.005%; Cr—0.04%; Mo—0.03%; Ni—1.31%; Fe—balance) were used in the present work. The specimens were degreased with acetone to remove impurities from the substrate. Then, the specimens were subjected to sand blasting at a pressure of 100 psi through the nozzle to get the appropriate crevices. The particle size of the sand was 80 mesh. The distance between the substrate and the blaster was maintained at 2 ft. The cleaned specimens prepared were kept in the desiccators for conditioning.

Preparation of neat CPBz and F-SiO_2–TiO_2-reinforced CPBz coatings

The neat CPBz and varying weight percentages of F-SiO_2–TiO_2-reinforced CPBz coatings were prepared by dip-coating method. CPBz monomer and 0, 1, 3, 5, and 7 wt% of F-SiO_2–TiO_2 were mixed separately using chloroform as a solvent and constant stirring for 2 h. The substrates were dip-coated into the formulation. Then, the residual solvent was removed by drying in a vacuum at 70°C for 3 h. Finally, the coated samples were cured stepwise at 120, 160, 200, and 220°C for 1 h each to obtain dark brown-colored film-coated specimens.[18,19] The coated substrates were preserved for corrosion studies.

Characterization

The FTIR spectrum was recorded on a PerkinElmer 6X FTIR spectrometer. About 100 mg of optical-grade KBr was ground with a sufficient quantity of the solid sample to make the wt% mixture for making KBr pellets. After the sample was loaded, a minimum of 16 scans were collected for each sample at a resolution of ± 4 cm^{-1}. The ^{1}HNMR and ^{13}CNMR spectra of benzoxazine monomers were recorded with a Bruker 300 MHz NMR spectrometer. Samples were diluted using deuterated chloroform ($CDCl_3$), and tetramethylsilane (TMS) was used as an internal standard.

The thermogravimetric analysis (TGA) was performed on a Netzsch STA 409 PC thermogravimetric analyzer. The instrument was calibrated with calcium oxalate and aluminum supplied by Netzsch. The samples (about 50 mg) were heated from ambient temperature to 800°C under a continuous flow of nitrogen (60 ml/min), at 10°C/min. Morphological studies were carried out by using SEM. SEM-EDAX of the samples was examined using a scanning electron microscope (SEM; JEOL JSM model 6360) attached with Horiba used to record the morphology and composition at 20 kV. Transmission electron microscope (TEM) analysis was carried out on TECNAI-G2 (model T-30) at an accelerating voltage of 300 kV.

Dynamic mechanical analyses (DMA) of the samples were performed with Model Q-800 TA Instruments to study their viscoelastic properties. The cured benzoxazine samples were cut into 20 mm $\times$ 5 mm $\times$ 1 mm dimension, then clamped onto the tension clamp of the instrument and scanned from 30°C to 200°C at a scanning rate of 3°C/min. The tanδ values were recorded at a constant linear frequency of 1 Hz and preload force of 0.01 N.

Electrochemical measurements were taken by CH Instruments CHI660D workstation with a three-electrode system, in which the coated sample acted as the working electrode, calomel as the reference electrode, and a mild steel plate as the counter electrode. The area of working electrode was ~ 5 cm^2. All coated specimens' corrosion resistivity study were performed using 3.5wt% aqueous NaCl solution at ambient temperature, and repeated at least three times to ensure repeatable results. The steel was polarized at ± 10 mV around its open-circuit potential (OCP) by an alternating current (AC) signal with its frequency ranging from 100 kHz to 10 MHz (10 points per decade).

Results and discussion

FTIR analysis

The FTIR spectrum of caprolactam diamine (CPA-NH_2) is presented in Fig. S1. The appearance of band at 3344 cm^{-1} is attributed to the N–H stretching vibration of primary amine. The appearance of peaks at 2917 and 1642 cm^{-1} was assigned to the stretching vibration modes of aliphatic CH_2 and amide C=O groups, respectively.[14,24,25] Figures S2 and S3 illustrate the FTIR spectra of benzoxazine monomers and polybenzoxazines, respectively. Figure S2 shows the FTIR spectra of benzoxazine monomers of phenol, 4-fluorophenol, and cardanol; from the spectra, the new peaks at 938 and 1112 cm^{-1} confirm the formation of benzoxazines. The peaks appearing at 1645 and 1534 cm^{-1} confirm the presence of 1, 2, 3-trisubstituted benzene ring in all the benzoxazine monomers. The peaks appearing at 2948 and 2877 cm^{-1} corresponded to CH_2 group of stretching vibration. The curing reaction of polybenzoxazine was further confirmed by FTIR analysis and is shown in Fig. S3. The disappearance of peak at 938 cm^{-1} confirms the occurrences of ring-opening polymerization in benzoxazine monomers. The formation of new peak at 1437 cm^{-1} confirms the presence of the tetra-substituted benzene rings in PBz matrices.

Figure S4 illustrates the FTIR spectra of synthesized SiO_2–TiO_2 and functionalized SiO_2–TiO_2. From the spectra, the peaks appearing at 3491 and 1550 cm^{-1} correspond to stretching and bending vibration of the N–H bond of aminosilane. The peak appearing at 1108 cm^{-1} represents the stretching vibrations of Ti–O–Si linkage. This ascertains that the amino groups are present on the surface of the SiO_2–TiO_2.[27]

FTIR spectra were also used to ascertain the curing reaction of neat polybenzoxazine and varying weight percentages of F-SiO_2–TiO_2-reinforced nanocomposites and are presented in Fig. S5. The disappearance of peak at 938 cm^{-1} infers the initiation of ring-opening polymerization in benzoxazine monomers. The new peak appearing at 1437 cm^{-1} confirms the presence of tetra-substituted benzene rings in CPBz matrices. The additional peak appearing at 951 cm^{-1} represents the Ti–O–Si linkage, which is absent in the case of neat polybenzoxazine.[28]

NMR analysis

^{1}H and ^{13}C NMR spectra of CPA-NH_2

Figures S6 and S7 illustrate the ^{1}H and ^{13}C NMR spectra of CPA-NH_2. The ^{1}H NMR spectrum and the aromatic protons appeared at 6.6 and 6.9 ppm, and amine proton appeared at 3.5 ppm. The methylene proton and aliphatic protons appeared at 3.0 and 1.6–2.4 ppm, respectively. In ^{13}C NMR, the carbonyl carbons appeared at 179 ppm, aromatic carbons appeared between 115 and 144 ppm and aliphatic carbons appeared between 23 and 42 ppm.[24,25]

^{1}H and ^{13}C NMR spectra of benzoxazine monomers

Figures S8–S13 show the ^{1}H and ^{13}C NMR spectra of benzoxazine monomers. The peaks appearing from

6.64 to 7.34 ppm were assigned to the aromatic protons. The peaks appearing at around 4.0 ppm and 5.0 ppm are assigned to –O–CH_2–N– and Ar–CH_2–N–, respectively. In ^{13}C NMR, the carbonyl carbon appeared at 180 ppm, aromatic carbons appeared from 115 to 144 ppm and aliphatic carbon atoms appeared from 14 to 36 ppm. The peak appearing at 130 ppm confirms the presence of vinyl carbon of long aliphatic side chain.[25] The peaks appearing at around 80.0 ppm and 60.0 ppm are assigned to –O–CH_2–N– and Ar–CH_2–N–, respectively.

XRD analysis

The polybenzoxazine network structure of 4-fluorophenol, phenol, and cardanol was characterized using XRD patterns and is presented in Fig. S14. The XRD pattern of polybenzoxazine exhibits an amorphous peak at 2θ=18.50 which corresponds to the characteristic peak of polybenzoxazine. The cardanol-based polybenzoxazine shows the reduced intensity and is due to the presence of long aliphatic chain present in it.

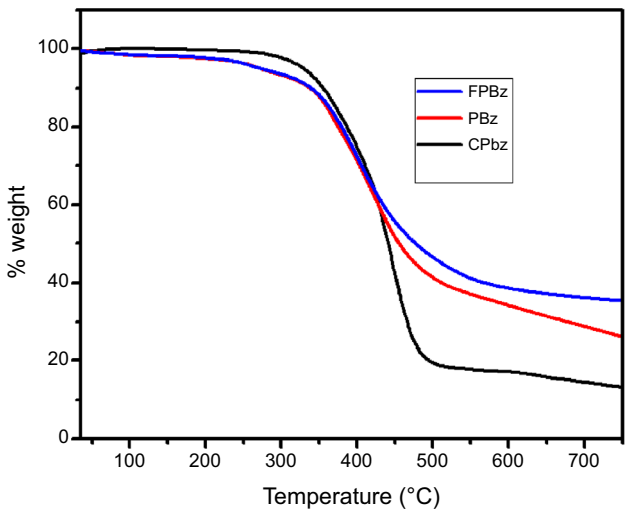

Fig. 1: TGA of polybenzoxazines of 4-fluorophenol, phenol, and cardanol

X-ray diffraction profiles of hybrid SiO_2–TiO_2 composites calcined at 600°C are shown in Fig. S15. In the XRD pattern, the typical amorphous peak appearing at around 2θ=21° was attributed to the amorphous SiO_2 matrix. The peaks located at 25.2°, 37.8°, 44.0°, 53.5°, 54.1°, and 64.2° correspond to the (101), (004), (200), (105), (211), and (204) planes of the anatase phase which in turn confirms the structure of synthesized SiO_2–TiO_2.[27,28]

Thermal properties

Thermogravimetric analysis

The thermal stability of polybenzoxazines was studied using TGA in the temperature range of 30–750°C. Data pertaining to the thermal stability of the polybenzoxazines are presented in Fig. 1 and Table 1. The degradation pattern was found varied with respect to the molecular structure of phenols which provides stability against the thermal degradation. From Fig. 1, 4-fluorophenol-based polybenzoxazine shows the higher char yield than that of conventional phenol and cardanol. The char yield values of phenol, 4-fluorophenol, and cardanol are 24%, 35%, and 22%, respectively. 4-Fluorophenol-based polybenzoxazine shows a higher char yield (35%), due to the presence of fluorine atom in the polybenzoxazine structure, and contributes to the higher thermal stability. The C–F bond is thermally more stable and stronger than that of the C–H bond. Thus, the presence of C–F bond contributes to retarded thermal degradation of benzoxazine moiety.

Figure 2 illustrates the TGAs of F-SiO_2–TiO_2-reinforced CPBz nanocomposites. The TGA was carried out to assess the thermal stability and high-temperature performance of these nanocomposites with reference to neat CPBz. TGAs of neat CPBz and F-SiO_2–TiO_2-reinforced CPBz nanocomposites samples demonstrate the substantial increase in thermal decomposition temperature when compared to that of neat CPBz. With the increasing weight percentages of F-SiO_2–TiO_2, the percentage of char yield also increased up to 5 wt% F-SiO_2–TiO_2; beyond 5 wt %, the value of char yield was not enhanced as expected. This may be attributed to the most likely phase separation between benzoxazine matrix and F-SiO_2–TiO_2 due to inefficient interfacial interactions.[29]

Table 1: Thermal properties and contact angle of polybenzoxazine

Sample	Weight loss (%)					Contact angle (θ)	
	10%	20%	30%	Char yield (%)	LOI	Water	DIM
PBz	335	373	400	24	27	81.9	60.4
CPBz	354	385	410	13	18	97.6	62.5
FPBz	339	378	407	35	31	116.0	65

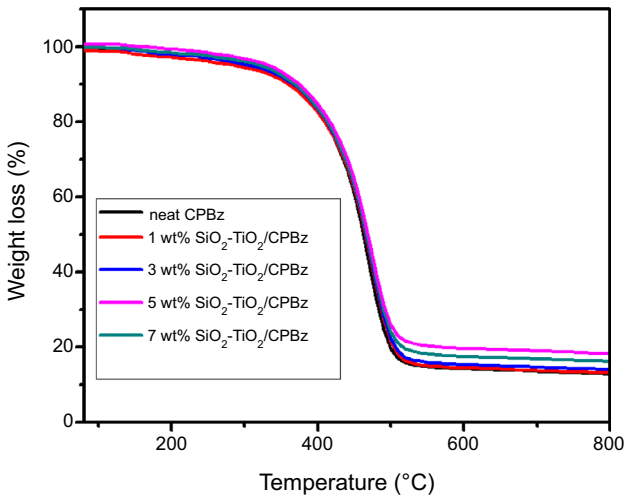

Fig. 2: TGA of (a) neat CPBz, (b) 1 wt% F-SiO_2–TiO_2/CPBz, (c) 3 wt% F-SiO_2–TiO_2/CPBz, (d) 5 wt% F-SiO_2–TiO_2/CPBz, and (e) 7 wt% F-SiO_2–TiO_2/CPBz

The phase separation between organic and inorganic phases cannot be avoided, though it may be restricted to a higher loading of inorganic filler by improving interphase interactions.

Figure S16 illustrates the DSC profile of 4-fluorophenol-, phenol-, and cardanol-based benzoxazines. On heating benzoxazine, the ring gets opened by the cleavage of C–O bond; thereby, the benzoxazine molecule is transformed from a ring structure to a linear open-chain structure. In this process, the trisubstituted benzene ring becomes the tetra-substituted, leading to the formation of polybenzoxazine, a phenol Mannich base. The glass transition temperature (T_g) of 4-fluorophenol-based benzoxazine is 165° C and is higher than that of other benzoxazines. This may be explained due to more electronegative nature of fluorine atom which restricts the segmental mobility. Cardanol-based benzoxazine exhibits a lower value of glass transition temperature (T_g) than that of other phenol-based benzoxazine systems, and the values are presented in Table 1. The decreased value of T_g is responsible for the plasticization effect of the cardanol. This may be explained due to the chain lengthening and flexibility behavior of long aliphatic chain in the cardanol moiety, which decreased the effective crosslink density. This creates an excess free volume in the matrix system and thus leads to the reduction in the value of T_g, of cured benzoxazine matrix. This result is in good agreement with the previous results reported for cardanol-based benzoxazines.[19,20] Their high flexibility and the presence of long aliphatic chain provides an enhanced free volume and decreased crosslink density, which in turn reduces the value of glass transition temperature.

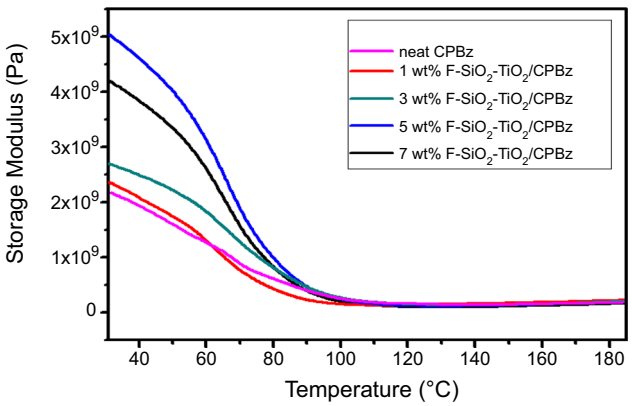

Fig. 3: Storage modulus of neat CPBz and varying weight percentages of F-SiO_2–TiO_2-reinforced CPBz composites

Flame-retardant properties

The flame-retardant properties of phenol-, 4-fluorophenol-, and cardanol-based polybenzoxazine are studied using the value of limiting oxygen index (LOI). The LOI value can be considered as an indicator to evaluate the flame retardancy of polymeric materials. The values of LOI calculated using equation (1) for PBz are presented in Table 1.[29,30]

$$\mathrm{LOI} = 17.5 + 0.4(\sigma) \quad (1)$$

where σ is char yield (data obtained from TGA) and the LOI values calculated are in the range of 26–31 (Table 1). The LOI values of the polymers should be above the threshold value of 26 to render them self-extinguishing and for their qualification for many applications requiring good flame resistance.

Dynamic mechanical analysis (DMA)

Storage modulus

Dynamic mechanical analysis (DMA) presents the information of the storage modulus (G') and tanδ in the test temperature range. The storage modulus represents the elastic property or the energy storage in the nanocomposites, and tanδ is often used to determine the glass transition temperature (T_g). From Fig. 3 and Table 2, the storage modulus of 1, 3, 5, and 7 wt% F-SiO_2–TiO_2-reinforced CPBz nanocomposites is 2373, 2719, 5038, and 4199 MPa, respectively, which are significantly higher than that of the neat CPBz (2175 MPa). The 7 wt% of F-SiO_2–TiO_2-reinforced CPBz nanocomposites exhibits lower storage modulus than composites with 5 wt% F-SiO_2–TiO_2. The enhancement of storage modulus may arise from the occurrence of an efficient interaction existing between

Table 2: Thermal and mechanical properties of neat CPBz and varying weight percentages of F-SiO_2–TiO_2-reinforced CPBz nanocomposites

Sample	Apparent crosslink density $\upsilon_e \times 10^5$ (mol m^{-3}) at 30°C	Storage modulus (MPa) at 30°C	Char yield % at 800°C	T_g (°C)	Contact angle (θ)
Neat CPBz	2.81	2175	11.8	94	97.6
1 wt% F-SiO_2–TiO_2/CPBz	3.06	2373	13.1	95	98.2
3 wt% F-SiO_2–TiO_2/CPBz	3.51	2719	14.5	98	102.8
5 wt% F-SiO_2–TiO_2/CPBz	6.57	5038	18.5	103	108.9
7 wt% F-SiO_2–TiO_2/CPBz	5.43	4199	15.8	100	113.4

the functionalized SiO_2–TiO_2 surface nanoparticles and CPBz. During the curing process, the functionalized SiO_2–TiO_2 not only reacts with the CPBz, but also interacts with the aminosilane groups present on F-SiO_2–TiO_2, forming the effective interfacial bonding, which in turn makes the better load transfer efficiency from the CPBz matrix to the rigid inorganic phase of F-SiO_2–TiO_2.[30–33] Hence, the nanocomposites possess the values of higher modulus even at the elevated temperatures.

The values of crosslink density of neat CPBz and apparent crosslink density[34,35] of F-SiO_2–TiO_2-filled CPBz nanocomposites are estimated using equation (2).

$$v_e = E'/3RT \tag{2}$$

where E' is a rubbery state modulus (Pa), R is the gas constant (8.314 cm^3 kPa/mol K), T is the temperature (°C) and ν_e is the crosslink density (10^5 mol/m^3).[36] The apparent crosslink density values of filled CPBz nanocomposites materials calculated are presented in Table 2. It can be seen that the value apparent crosslink density is obviously increased with increasing the wt% of F-SiO_2–TiO_2-reinforced CPBz composites and the values obtained for 1, 3, and 5 wt% are 3.06, 3.51, and 6.57×10^5 mol/m^3, respectively. The enhanced apparent crosslink density may be explained due to the result of efficient interaction occurring between F-SiO_2–TiO_2 and CPBz matrix. Further, as observed in the case of value of storage modulus for 7 wt% F-SiO_2–TiO_2-reinforced CPBz nanocomposites, the value of apparent crosslink density also decreased calculated at 5.43×10^5 mol/m^3. At higher concentration of 7 wt% F-SiO_2–TiO_2-reinforced CPBz composites, the reinforcement particles are dispersed irregularly (agglomeration) into the CPBz matrix and retard the effective formation of network structure, which in turn leads to a decrease in the value of apparent crosslink density. Further, the SEM image observed also supports and infers the evidence for agglomeration of 7 wt% F-SiO_2–TiO_2-reinforced CPBz composites. Thus, beyond 7 wt% of reinforcement lowers both the values of storage modulus and apparent crosslink density.

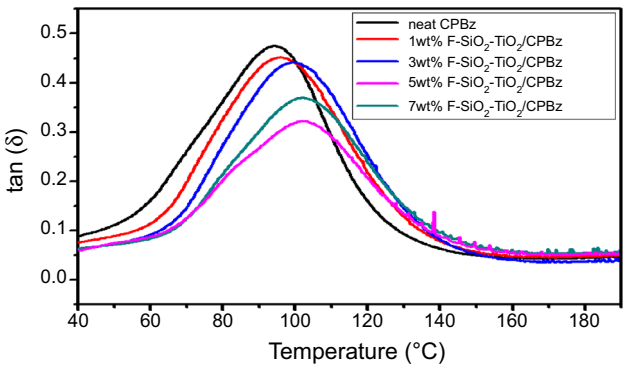

Fig. 4: Glass transition temperatures of the neat CPBz and varying weight percentages of F-SiO_2–TiO_2-reinforced CPBz nanocomposites

Glass transition temperature

The tanδ is the ratio of the loss modulus to the storage modulus, and the peak of tanδ is often used to determine the glass transition temperature (T_g). The value of T_g obtained is presented in Fig. 4 and Table 2. On increasing the weight percentage of F-SiO_2–TiO_2, the values of T_g increase to 95, 98, and 103°C for 1, 3, and 5 wt%, respectively. The value of T_g shows an increasing trend, and this is perhaps attributed to the effective interaction results between the surfaces of the reinforcement and matrix, which restricted the chain mobility of CPBz segments. Further, the rigid inorganic materials of F-SiO_2–TiO_2 incorporated into the CPBz matrix crosslinked network structure and enhanced the value of T_g. However, it was noticed that the value of T_g decreased for 7 wt% of F-SiO_2–TiO_2-reinforced CPBz nanocomposites to 100°C, due to the creation of excess free volume by F-SiO_2–TiO_2, which in turn imparts flexibility, thus resulting in lowering of T_g. The reduction in tanδ peak is consistent with the increase in T_g as it is seen in the DMA measurements, and this may be related to the occurrence of interfacial interaction between the polymer chains and F-SiO_2–TiO_2 at low level of loading up to 5 wt%. On the other hand, beyond 5 wt% F-SiO_2–TiO_2 loading, the value of T_g is decreased due to particle agglomeration.[33]

Morphological studies

SEM analysis

The elemental composition of PBz, CPBz, and FPBz was confirmed using the energy-dispersive X-ray spectra (EDAX), integrated with scanning electron microscopy analysis, and is shown in Fig. 5. From the spectrum, the appropriate elemental composition of carbon, nitrogen, oxygen, and fluorine present in the polybenzoxazines is ascertained.

SEM images of neat CPBz and 1, 3, 5, and 7 wt% of F-SiO_2–TiO_2-reinforced CPBz nanocomposites are shown in Fig. 6. The neat CPBz matrix shows smooth and clear images without any particles. The 1, 3, and 5 wt% of F-SiO_2–TiO_2-reinforced CPBz nanocomposites show the uniform- and molecular-level dispersion of F-SiO_2–TiO_2 into CPBz matrix.[24] The 7 wt% of F-SiO_2–TiO_2-reinforced CPBz nanocomposites shows the agglomeration of F-SiO_2–TiO_2 into CPBz matrix.[24] The elemental composition of neat CPBz and 7 wt% of F-SiO_2–TiO_2-reinforced CPBz nanocomposites was confirmed with the energy-dispersive X-ray spectral (EDS) analysis and is shown in Fig. 7a and 7b. From the spectrum, it was found that the appropriate concentration of Ti, Si, and other polymer backbones is present in the nanocomposites.

TEM analysis

The morphology of developed F-SiO_2–TiO_2-reinforced CPBz nanocomposites was further confirmed with TEM analysis, and the images are presented in Fig. 8. The synthesized hybrid SiO_2–TiO_2 nanoparticles are shown in Fig. 6a. From the TEM image, the black regions indicate the presence of TiO_2 over the surface of SiO_2 layer. Figure 6b shows the image of 5 wt% F-

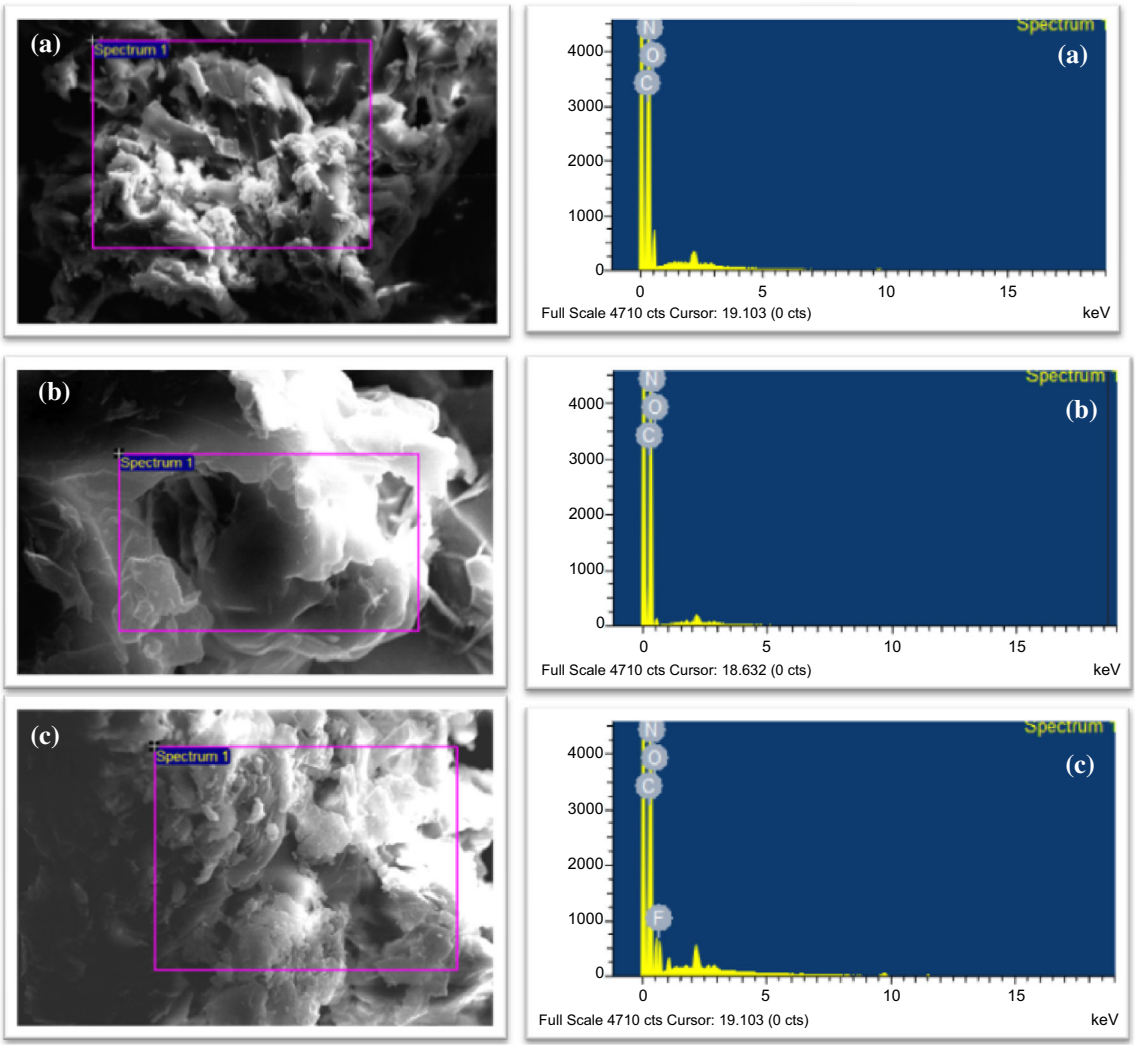

Fig. 5: SEM-EDX images of polybenzoxazine of (a) PBz, (b) CPBz, and (c) FPBz

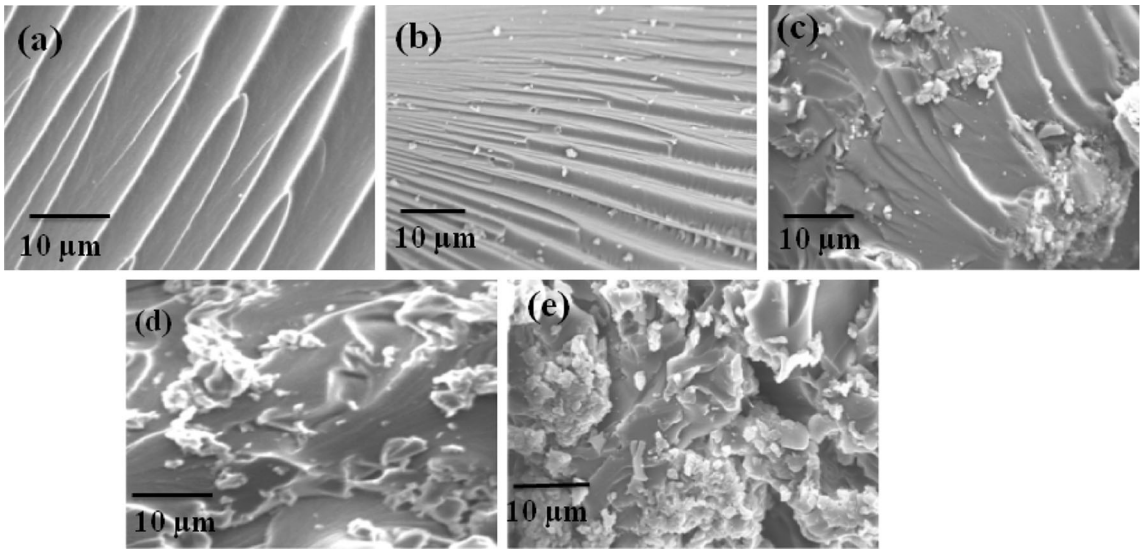

Fig. 6: SEM micrograph of (a) neat CPBz, (b) 1 wt% F-SiO_2–TiO_2/CPBz, (c) 3 wt% F-SiO_2–TiO_2/CPBz, (d) 5 wt% F-SiO_2–TiO_2/CPBz, and (e) 7 wt% F-SiO_2–TiO_2/CPBz

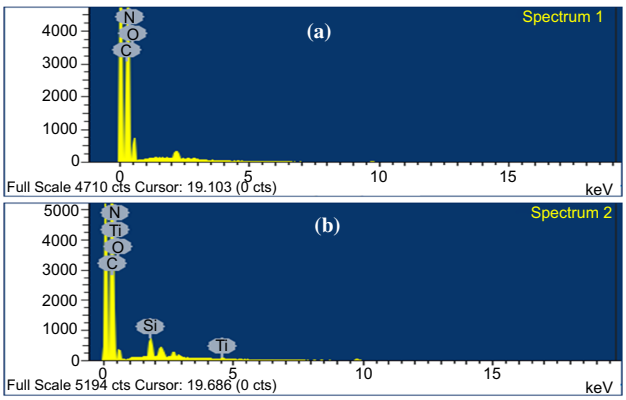

Fig. 7: EDS spectrum of neat and 7 wt% of F-SiO_2–TiO_2-reinforced CPBz nanocomposites

SiO_2–TiO_2-reinforced CPBz nanocomposites, which ascertains the existence of effective interfacial interaction between the F-SiO_2–TiO_2 and CPBz matrix is well demonstrated, and also indicates the homogeneous dispersion of F-SiO_2–TiO_2 with CPBz nanocomposites.

Contact angle studies

Table 1 shows the list of the surface contact angle images of polybenzoxazines synthesized from phenol, 4-fluorophenol, and cardanol. It has been established experimentally that the value of contact angle is influenced by the roughness of the surface in accordance with the Wenzel or Cassie–Baxter model and is dependent upon whether the surface is hydrophilic or hydrophobic. The value of surface contact angle is measured with 5 ml of water and diiodomethane as the probe liquids, and the results obtained are presented in Table 1. The values of contact angle for PBz, CPBz, and FPBz in water are 81.9, 83.3, and 116.0, respectively, and those of diiodomethane (DIM) are 60.4, 62.5, and 65, respectively.

Polybenzoxazines having strong intramolecular hydrogen bonding contribute to the lower surface free energy. The polybenzoxazine synthesized from 4-fluorophenol possesses the higher contact angle value than that of phenol and cardanol. This is due to the presence of highly electronegative fluorine atom in the benzoxazine skeleton which increases the hydrophobicity with lowering the value of surface free energy.

Cardanol has a long aliphatic side chain at meta position, and it influences an enhanced water contact angle. Cardanol-based benzoxazine exhibits a higher value of contact angle than that of phenol-based benzoxazine and is also more cost competitive than that of 4-fluorophenol. Further, cardanol is a bio-based material, and the present work is mainly focused on biomaterial-based coating materials for corrosion resistance application toward the protection of mild steel specimen. The values of contact angle obtained for 1, 3, 5, and 7 wt% SiO_2–TiO_2-reinforced CPBz composites are 98.2°, 102.8°, 108.9°, and 113.4°,[31–33] respectively (Table 2).

Corrosion resistance analysis

The corrosion-resistant properties of the neat CPBz and varying weight percentages of F-SiO_2–TiO_2-reinforced CPBz-coated specimens of MS plate were

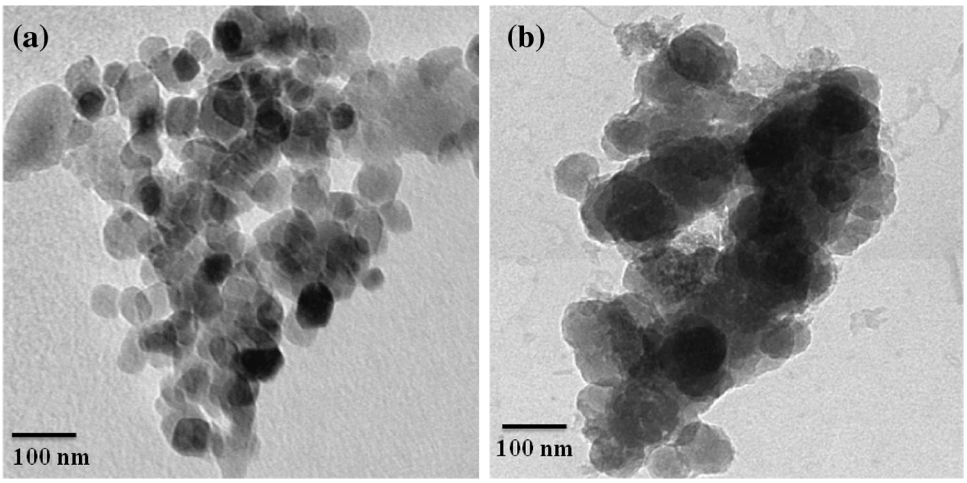

Fig. 8: TEM micrograph of (a) SiO_2–TiO_2 nanoparticles and (b) 5 wt% F-SiO_2–TiO_2/CPBz nanocomposites

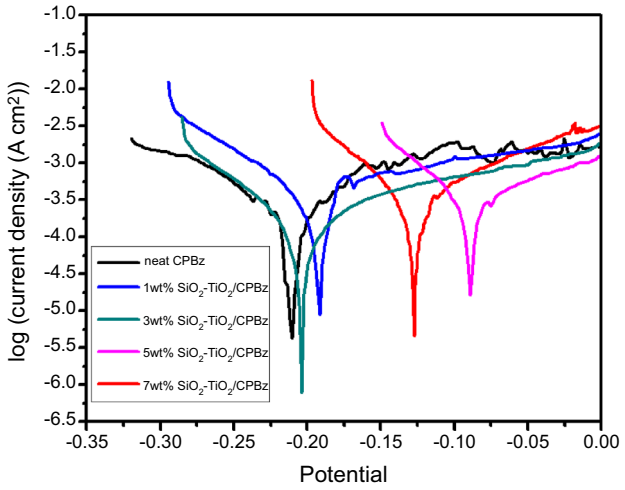

Fig. 9: Tafel plots of coated specimens of the neat CPBz and varying weight percentages of F-SiO_2–TiO_2-reinforced CPBz immersed in 3.5 wt% NaCl aqueous solution

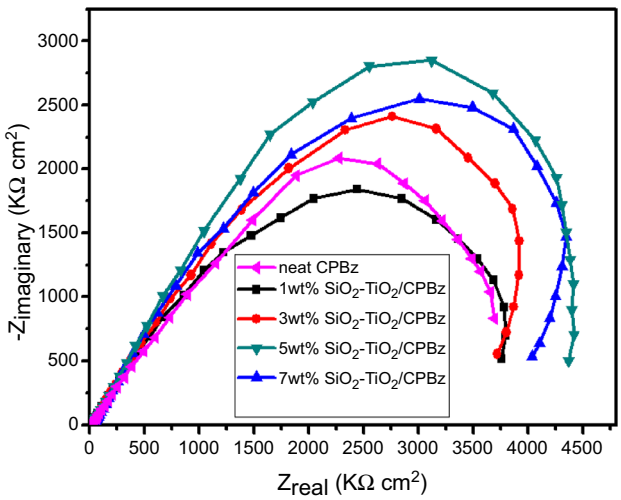

Fig. 10: Nyquist plots of coated specimens of the neat CPBz and varying weight percentages of F-SiO_2–TiO_2-reinforced CPBz immersed in 3.5 wt% NaCl aqueous solution

carried out in 3.5 wt% NaCl aqueous solutions by using electrochemical work station. F-SiO_2–TiO_2-reinforced CPBz-coated specimens were investigated in detail by polarization and EIS techniques. Figure 9 exhibits Tafel plots which show a remarkable shift toward positive potential for the CPBz with different wt% loadings of F-SiO_2–TiO_2-coated specimens as compared to that of CPBz-coated specimen. It was noticed that 5 wt% of F-SiO_2–TiO_2-reinforced CPBz nanocomposite-coated specimen shows better corrosion resistance than 7 wt% of F-SiO_2–TiO_2-reinforced CPBz nanocomposite-coated specimen.

Electrochemical impedance spectroscopy (EIS) is a nondestructive electrochemical method used to estimate the performance of the coatings against corrosion. The properties of the coating sample can be differentiated from the frequency capacitance behavior obtained from Nyquist plots (Fig. 10). The Nyquist plots for F-SiO_2–TiO_2-reinforced CPBz nanocomposite-coated specimens show much higher corrosion resistance behavior when compared to that of neat CPBz-coated specimen. The high-frequency capacitance behavior of the coated specimen of 5 wt% F-SiO_2–TiO_2-reinforced CPBz nanocomposites demonstrates the highest corrosion resistance behavior, while low-frequency capacitance behavior indicates the occurrence of capacitance process at the coating/metal interface.[18,19,37,38]

From the results of electrochemical measurements, it is clear that the F-SiO_2–TiO_2-reinforced CPBz nanocomposite materials possess a significant improvement in the corrosion-resistant properties when compared with that of conventional benzoxazine coatings in 3.5% NaCl solution. However, it is necessary to evaluate the corrosion resistance of the coating for relatively longer period of exposure to corrosive electrolyte. Data obtained from corrosion studies inferred that the benzoxazine sample CPBz with 5 wt % loading of F-SiO_2–TiO_2 has shown the superior corrosion resistance among the F-SiO_2–TiO_2-reinforced CPBz specimens studied.

Conclusion

Cardanol, a well-known by-product of the cashew industry, has been used for the synthesis of benzoxazine monomer. Silica and titania were chemically synthesized and were introduced into cardanol-based polybenzoxazine to obtain nanocomposites to enhance the anticorrosive behavior and mechanical properties of coatings. FTIR, NMR, DSC, TGA, XRD, SEM-EDS, and TEM were used to characterize the prepared nanocomposites. The introduction of the F-SiO_2–TiO_2 inorganic phase into CPBz resin improved T_g and thermomechanical properties. The results showed that there was a significant improvement in the coating performance due to the incorporation of F-SiO_2–TiO_2. However, the 7 wt % of F-SiO_2–TiO_2-reinforced CPBz composites show lower T_g and lower storage modulus than those of other composite samples due to irregular dispersion of particles in the matrix which is also evidenced from SEM image. Data obtained from corrosion resistance analysis carried out on mild steel specimen indicate that 5 wt% F-SiO_2–TiO_2-reinforced CPBz composites possess better corrosion-resistant behavior than that of neat CPBz. Data resulted from different studies suggested that these hybrid F-SiO_2–TiO_2-reinforced CPBz composites can be used as coating materials for enhanced performance and improved longevity.

References

1. Foyet, A, Wu, TH, van der Ven, L, Kodentsov, A, de With, G, van Benthem, R, "Influence of Mixing Ratio on the Permeability of Water and the Corrosion Performance of Epoxy/Amine Coated Un-pretreated Al-2024 Evaluated by Impedance Spectroscopy." *Prog. Org. Coat.*, **64** 138–141 (2009)
2. Meis, NN, van der Ven, LG, van Benthem, RA, de With, G, "Extreme Wet Adhesion of a Novel Epoxy-Amine Coating on Aluminum Alloy 2024-T3." *Prog. Org. Coat.*, **77** (1) 176–183 (2014)
3. Ishida, H, Allen, DJ, "Physical and Mechanical Characterization of Near-Zero Shrinkage Polybenzoxazines." *J. Polym. Sci. Part B Polym. Phys.*, **34** (6) 1019–1030 (1996)
4. Arumugam, H, Krishnan, S, Chavali, M, Muthukaruppan, A, "Cardanol Based Benzoxazine Blends and Bio-silica Reinforced Composites: Thermal and Dielectric Properties." *New J. Chem.*, **42** (6) 4067–4080 (2018)
5. Ariraman, M, Alagar, M, "Design of Lamellar Structured POSS/BPZ Polybenzoxazine Nanocomposites as a Novel Class of Ultra Low-k Dielectric Materials." *RSC Adv.*, **4** (37) 19127–19136 (2014)
6. Ishida, H, Rodriguez, Y, "Curing Kinetics of a New Benzoxazine-Based Phenolic Resin by Differential Scanning Calorimetry." *Polymer*, **36** (16) 3151–3158 (1995)
7. Ghosh, NN, Kiskan, B, Yagci, Y, "Polybenzoxazines—New High Performance Thermosetting Resins: Synthesis and Properties." *Prog. Polym. Sci.*, **32** (11) 1344–1391 (2007)
8. Dumas, L, Bonnaud, L, Olivier, M, Poorteman, M, Dubois, P, "Facile Preparation of a Novel High Performance Benzoxazine–CNT Based Nano-hybrid Network Exhibiting Outstanding Thermo-mechanical Properties." *Chem. Commun.*, **49** (83) 9543–9545 (2013)
9. Huang, K, Zhang, Y, Li, M, Lian, J, Yang, X, Xia, J, "Preparation of a Light Color Cardanol-Based Curing Agent and Epoxy Resin Composite: Cure-Induced Phase Separation and Its Effect on Properties." *Prog. Org. Coat.*, **74** (1) 240–247 (2012)
10. Sultania, M, Rai, JS, Srivastava, D, "Process Modeling, Optimization and Analysis of Esterification Reaction of Cashew Nut Shell Liquid (CNSL)-Derived Epoxy Resin Using Response Surface Methodology." *J. Hazard. Mater.*, **185** (2–3) 1198–1204 (2011)
11. Ikeda, R, Tanaka, H, Uyama, H, Kobayashi, S, "Synthesis and Curing Behaviors of a Crosslinkable Polymer from Cashew Nut Shell Liquid." *Polymer*, **43** (12) 3475–3481 (2002)
12. Balgude, D, Sabnis, AS, "CNSL: An Environment Friendly Alternative for the Modern Coating Industry." *J. Coat. Technol. Res.*, **11** (2) 169–183 (2014)
13. Xu, GM, Shi, T, Liu, J, Wang, Q, "Preparation of a Liquid Benzoxazine Based on Cardanol and the Thermal Stability of Its Graphene Oxide Composites." *J. Appl. Polym. Sci.*, **131** (11) 40353–40361 (2014)
14. Sethuraman, K, Alagar, M, "Thermo-mechanical and Dielectric Properties of Graphene Reinforced Caprolactam Cardanol Based Benzoxazine–Epoxy Nanocomposites." *RSC Adv.*, **5** (13) 9607–9617 (2014)
15. Liu, L, Hu, JM, Leng, WH, Zhang, JQ, Cao, CN, "Novel Bis-silane/TiO_2 Bifunctional Hybrid Films for Metal Corrosion Protection Both Under Ultraviolet Irradiation and in the Dark." *Scr. Mater.*, **57** (6) 549–552 (2007)
16. Shen, GX, Chen, YC, Lin, CJ, "Corrosion Protection of 316 L Stainless Steel by a TiO_2 Nanoparticle Coating Prepared by Sol–Gel Method." *Thin Solid Films*, **489** (1–2) 130–136 (2005)
17. Jalili, MM, Moradian, S, Dastmalchian, H, Karbasi, A, "Investigating the Variations in Properties of 2-Pack Polyurethane Clear Coat through Separate Incorporation of Hydrophilic and Hydrophobic Nano-silica." *Prog. Org. Coat.*, **59** (1) 81–87 (2007)
18. Zhou, C, Lu, X, Xin, Z, Liu, J, Zhang, Y, "Polybenzoxazine/SiO_2 Nanocomposite Coatings for Corrosion Protection of Mild Steel." *Corros. Sci.*, **80** 269–275 (2014)
19. Zhou, C, Lu, X, Xin, Z, Liu, J, "Corrosion Resistance of Novel Silane-Functional Polybenzoxazine Coating on Steel." *Corros. Sci.*, **70** 145–151 (2013)
20. Yang, LH, Liu, FC, Han, EH, "Effects of P/B on the Properties of Anticorrosive Coatings with Different Particle Size." *Prog. Org. Coat.*, **53** (2) 91–98 (2005)

21. Ramezanzadeh, B, Attar, MM, "An Evaluation of the Corrosion Resistance and Adhesion Properties of an Epoxy-Nanocomposite on a Hot-Dip Galvanized Steel (HDG) Treated by Different Kinds of Conversion Coatings." *Surf. Coat. Technol.*, **205** (19) 4649–4657 (2011)
22. Behzadnasab, M, Mirabedini, SM, Kabiri, K, Jamali, S, "Corrosion Performance of Epoxy Coatings Containing Silane Treated ZrO_2 Nanoparticles on Mild Steel in 3.5% NaCl Solution." *Corros. Sci.*, **53** (1) 89–98 (2011)
23. Dhoke, SK, Khanna, AS, "Effect of Nano-Fe_2O_3 Particles on the Corrosion Behavior of Alkyd Based Waterborne Coatings." *Corros. Sci.*, **51** (1) 6–20 (2009)
24. Lakshmikandhan, T, Alagar, M, "Development and Characterization of Functionalized TiO_2-Reinforced Schiff Base Epoxy Nanocomposites." *High Perform. Polym.*, **27** (7) 813–823 (2015)
25. Selvaraj, V, Jayanthi, KP, Lakshmikandhan, T, Alagar, M, "Development of a Polybenzoxazine/TSBA-15 Composite from the Renewable Resource Cardanol for Low-k Applications." *RSC Adv.*, **5** (60) 48898–48907 (2015)
26. Thiripuranthagan, S, Raj, D, Kannan, K, "Photocatalytic Degradation of Congored on Silica Supported Ag Impregnated TiO_2." *J. Nanosci. Nanotechnol.*, **15** (6) 4727–4733 (2015)
27. Riazian, M, Bahari, A, "Synthesis and Nanostructural Investigation of TiO_2 Nanorods Doped by SiO_2." *Pramana*, **78** (2) 319–331 (2012)
28. Zhang, X, Zheng, H, "Synthesis of TiO_2-Doped SiO_2 Composite Films and Its Applications." *Bull. Mater. Sci.*, **31** (5) 787–790 (2008)
29. Rubab, Z, Afzal, A, Siddiqi, HM, Saeed, S, "Preparation, Characterization, and Enhanced Thermal and Mechanical Properties of Epoxy-Titania Composites." *Sci. World J.*, **1** 1–7 (2014). https://doi.org/10.1155/2014/515739
30. Takeichi, T, Kawauchi, T, Agag, T, "High Performance Polybenzoxazines as a Novel Type of Phenolic Resin." *Polym. J.*, **40** (12) 1121–1131 (2008)
31. Rajabi, L, Mohammadi, Z, Derakhshan, AA, "Thermal Stability and Dynamic Mechanical Properties of Nano and Micron-TiO_2 Particles Reinforced Epoxy Composites: Effect of Mixing Method." *Iran. J. Chem. Eng.*, **10** 16–29 (2013)
32. Liu, M, Guo, B, Du, M, Lei, Y, Jia, D, "Natural Inorganic Nanotubes Reinforced Epoxy Resin Nanocomposites." *J. Polym. Res.*, **15** (3) 205–212 (2008)
33. Mandhakini, M, Lakshmikandhan, T, Chandramohan, A, Alagar, M, "Effect of Nanoalumina on the Tribology Performance of C4-Ether-Linked Bismaleimide-Toughened Epoxy Nanocomposites." *Tribol. Lett.*, **54** (1) 67–79 (2014)
34. Fei, Z, Long, C, Qingyan, P, Shugao, Z, "Influence of Carbon Black on Crosslink Density of Natural Rubber." *J. Macromol. Sci. Part B Phys.*, **51** 1208–1217 (2012)
35. Xu, SH, Gu, J, Luo, YF, Jia, DM, "Effects of Partial Replacement of Silica with Surface Modified Nanocrystalline Cellulose on Properties of Natural Rubber Nanocomposites." *Express Polym. Lett.*, **6** (1) 14–25 (2012)
36. Thirukumaran, P, Shakila Parveen, A, Sarojadevi, M, Kim, SC, "Replacing Bisphenol-A with Bisguaiacol-F to Synthesize Polybenzoxazines for Pollution-Free Environment." *New J. Chem.*, **40** 9313–9319 (2016)
37. Escobar, J, Poorteman, M, Dumas, L, Bonnaud, L, Dubois, P, Olivier, MG, "Thermal Curing Study of Bisphenol A Benzoxazine for Barrier Coating Applications on 1050 Aluminum Alloy." *Prog. Org. Coat.*, **79** 53–61 (2015)
38. Fina, A, Tabuani, D, Frache, A, Camino, G, "Polypropylene–Polyhedral Oligomeric Silsesquioxanes (POSS) Nanocomposites." *Polymer*, **46** (19) 855–866 (2005)